Electronic Supplementary Information (ESI)

for

Flexible, linear, tetranuclear palladium complexes supported by tetraphosphine ligands with electron-withdrawing groups

Tomoaki Tanase,* Satoko Hatada, Ayaka Mochizuki, Kanako Nakamae, Bunsho Kure and Takayuki Nakajima

Department of Chemistry, Faculty of Science, Nara Women's University,

Kitauoya-nishi-machi, Nara 630-8506, Japan

E-mail: tanase@cc.nara-wu.ac.jp

Fig. S1. $^{31}P\{^{1}H\}$ NMR spectrum of dpmppmF$_2$ in $CDCl_3$ (b) with a simulated spectrum (a).

Fig. S2 $^{31}P\{^{1}H\}$ NMR spectrum of **5** in CD_2Cl_2 at room temperature.

Fig. S3. Variable−temperature UV−vis absorption spectra of **6** in CH_2Cl_2.

Fig. S4. Variable−temperature UV−vis absorption spectra of **3** in CH_2Cl_2.

Fig. S5. ^{19}F NMR spectra for the dpmppmF$_2$ region of **1** at −80 ºC in CD_2Cl_2 (a) and at 60 ºC in CD_3CN (b).

Fig. S6. Temperature−dependent (a) $^{31}P\{^{1}H\}$, (b) ^{1}H and (c) ^{19}F NMR spectra of **2** in CD_2Cl_2 (−80ºC < T < 20 ºC).

Fig. S7. Temperature−dependent (a) $^{31}P\{^{1}H\}$, (b) ^{1}H and (c) ^{19}F NMR spectra of **4** in CD_2Cl_2 (−80ºC < T < 20 ºC)

Fig. S8. Temperature−dependent (a) $^{31}P\{^{1}H\}$, (b) ^{1}H and (c) ^{19}F NMR spectra of **3** in CD_2Cl_2 (−80ºC < T < 20 ºC)

Fig. S9 DFT optimized structures of (a) $[Pd_4(\mu\text{–dpmppmF}_2)_2(XylNC)_3]^{2+}$ (**1**) and (b) $[Pd_4(\mu\text{–dpmppmF}_2)_2(XylNC)_2]^{2+}$ (**1'**) with selected structural parameters. DFT calculations were performed with B3LYP/lanl2dz methods.

Fig. S10 Values of natural charge (red) and Wiberg bond indices (blue) derived from Natural Bond Analyses on the DFT optimized structures of (a) $[Pd_4(\mu\text{–dpmppmF}_2)_2(XylNC)_3]^{2+}$ (**1**) and (b) $[Pd_4(\mu\text{–dpmppmF}_2)_2(XylNC)_2]^{2+}$ (**1'**).

Fig. S1. $^{31}P\{^{1}H\}$ NMR spectrum of dpmppmF$_2$ in $CDCl_3$ (b) with a simulated spectrum (a).

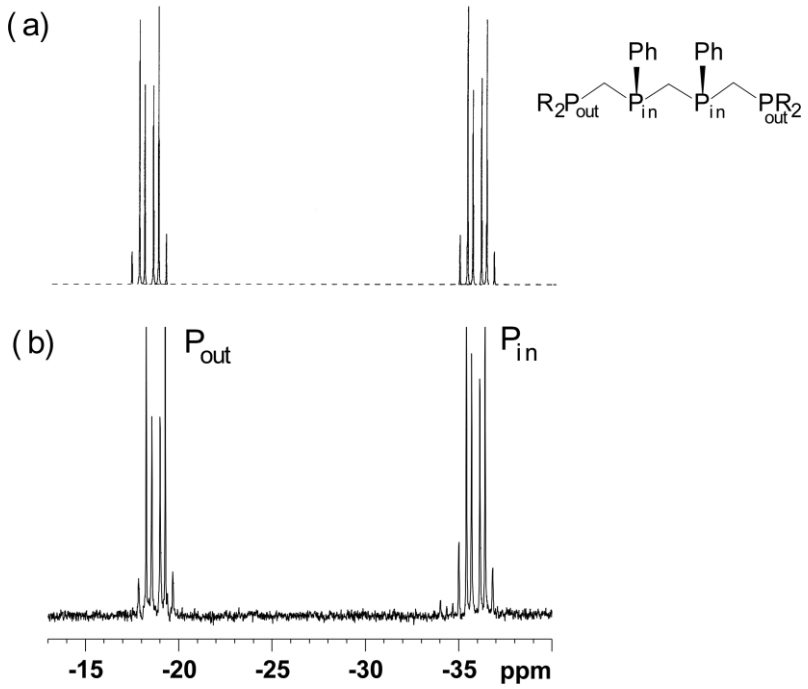

Fig. S2 $^{31}P\{^{1}H\}$ NMR spectrum of **5** in CD_2Cl_2 at room temperature.

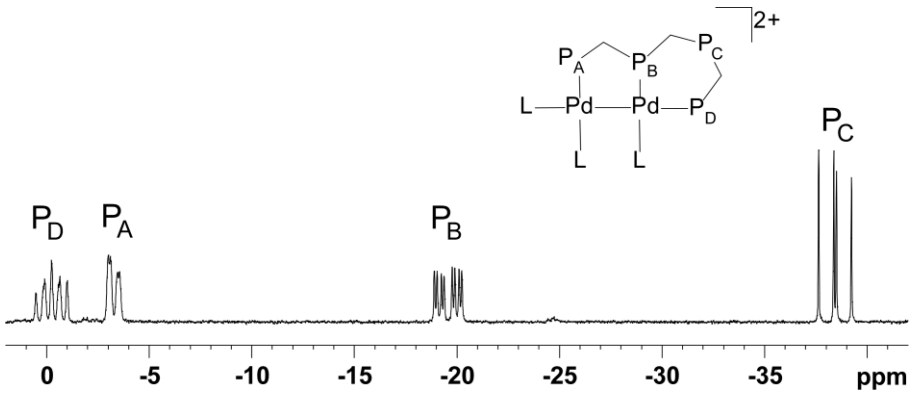

Fig. S3. Variable–temperature UV–vis absorption spectra of **6** in CH_2Cl_2.

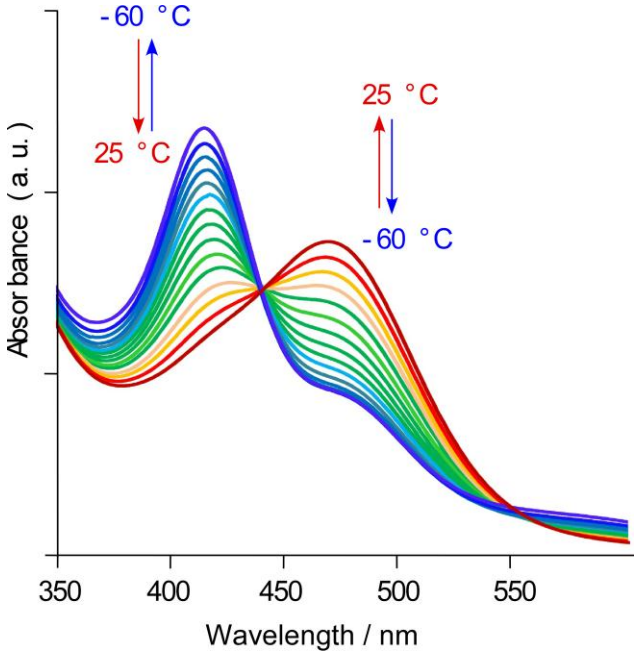

Fig. S4. Variable–temperature UV–vis absorption spectra of **3** in CH_2Cl_2.

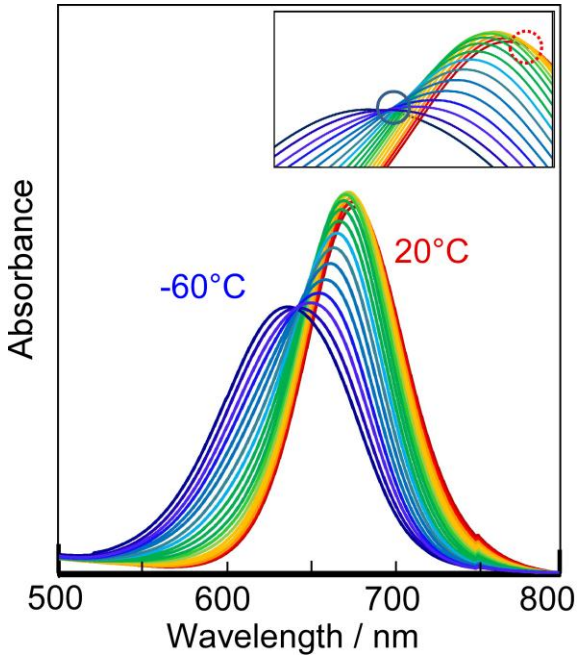

Fig. S5. ^{19}F NMR spectra for the dpmppmF_2 region of **1** at –80 ºC in CD_2Cl_2 (a) and at 60 ºC in CD_3CN (b).

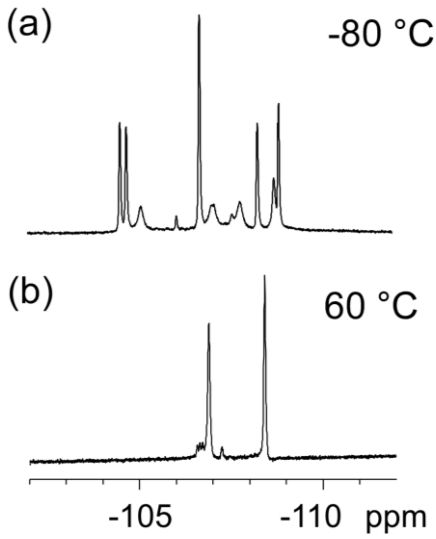

Fig. S6. Temperature–dependent (a) $^{31}P\{^1H\}$, (b) ^1H and (c) ^{19}F NMR spectra of **2** in CD_2Cl_2 (–80ºC < T < 20 ºC). The asterisks indicate impurity.

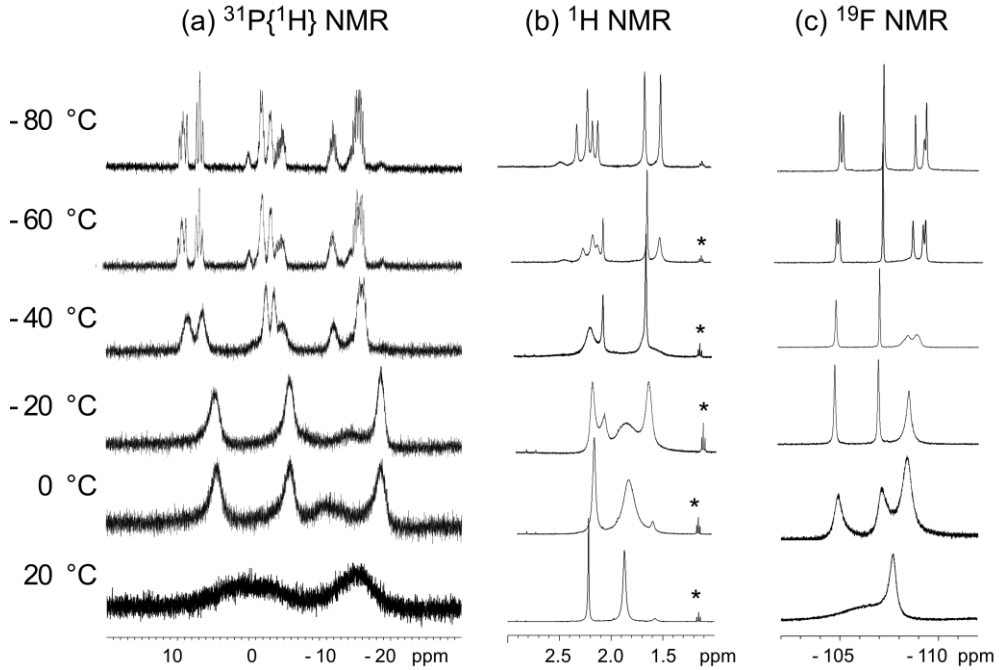

Fig. S7. Temperature–dependent (a) $^{31}P\{^{1}H\}$, (b) ^{1}H and (c) ^{19}F NMR spectra of **4** in CD_2Cl_2 (–80ºC < T < 20 ºC). The asterisks indicate impurity.

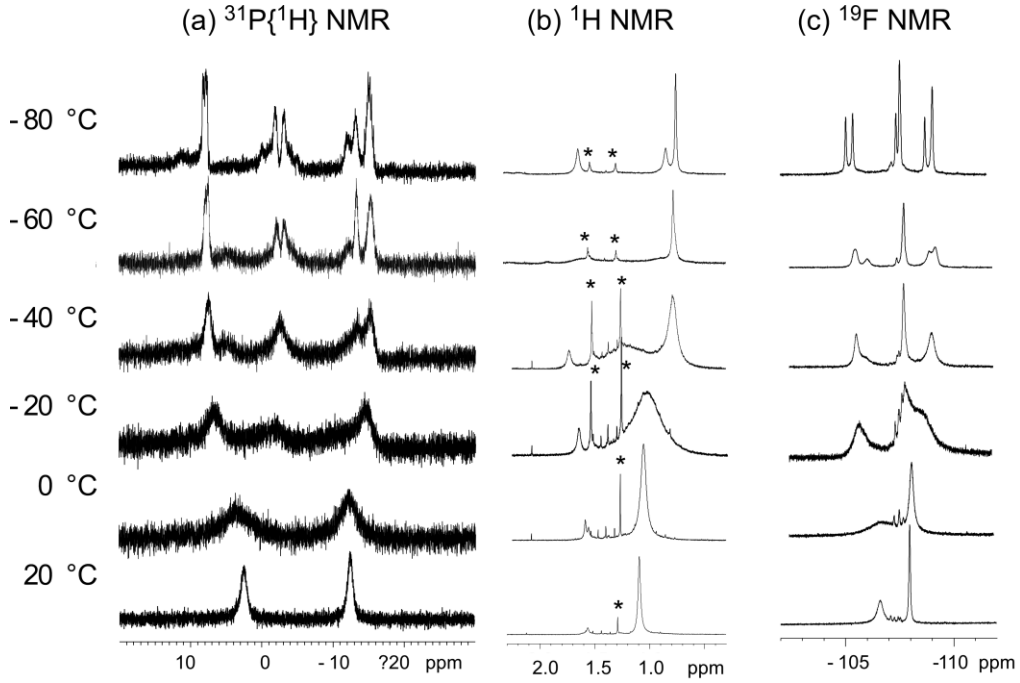

Fig. S8. Temperature–dependent (a) $^{31}P\{^{1}H\}$, (b) ^{1}H and (c) ^{19}F NMR spectra of **3** in CD_2Cl_2 (–80ºC < T < 20 ºC). The asterisks indicate impurity.

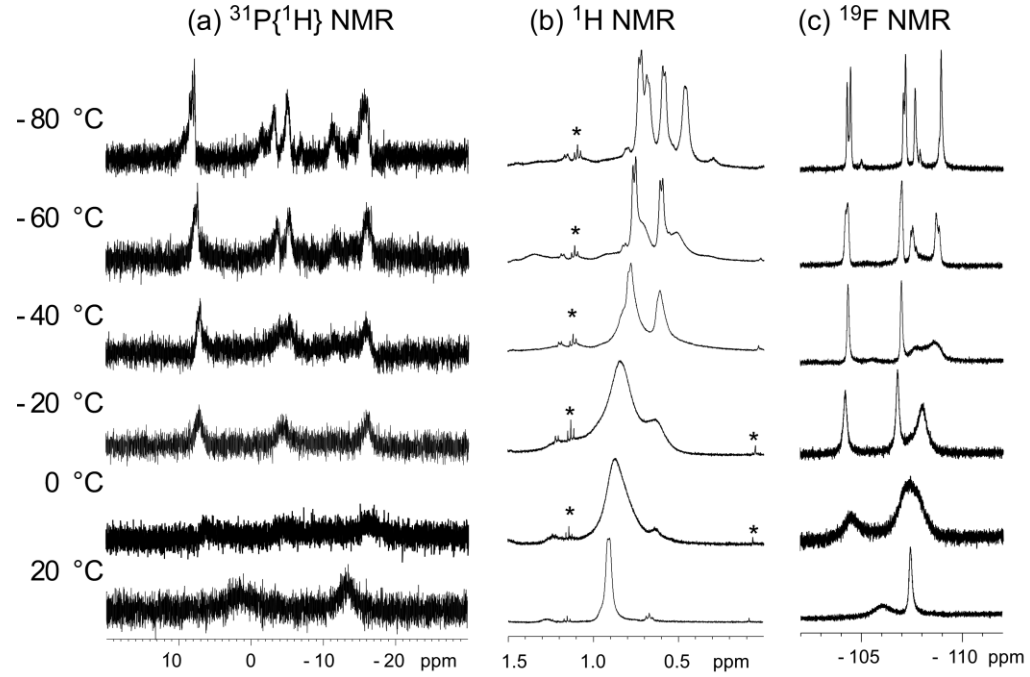

Fig. S9 DFT optimized structures of (a) $[Pd_4(\mu\text{–dpmppmF}_2)_2(XylNC)_3]^{2+}$ (**1**) and (b) $[Pd_4(\mu\text{–dpmppmF}_2)_2(Xyl\text{-}NC)_2]^{2+}$ (**1'**) with selected structural parameters. DFT calculations were performed with B3LYP/lanl2dz methods.

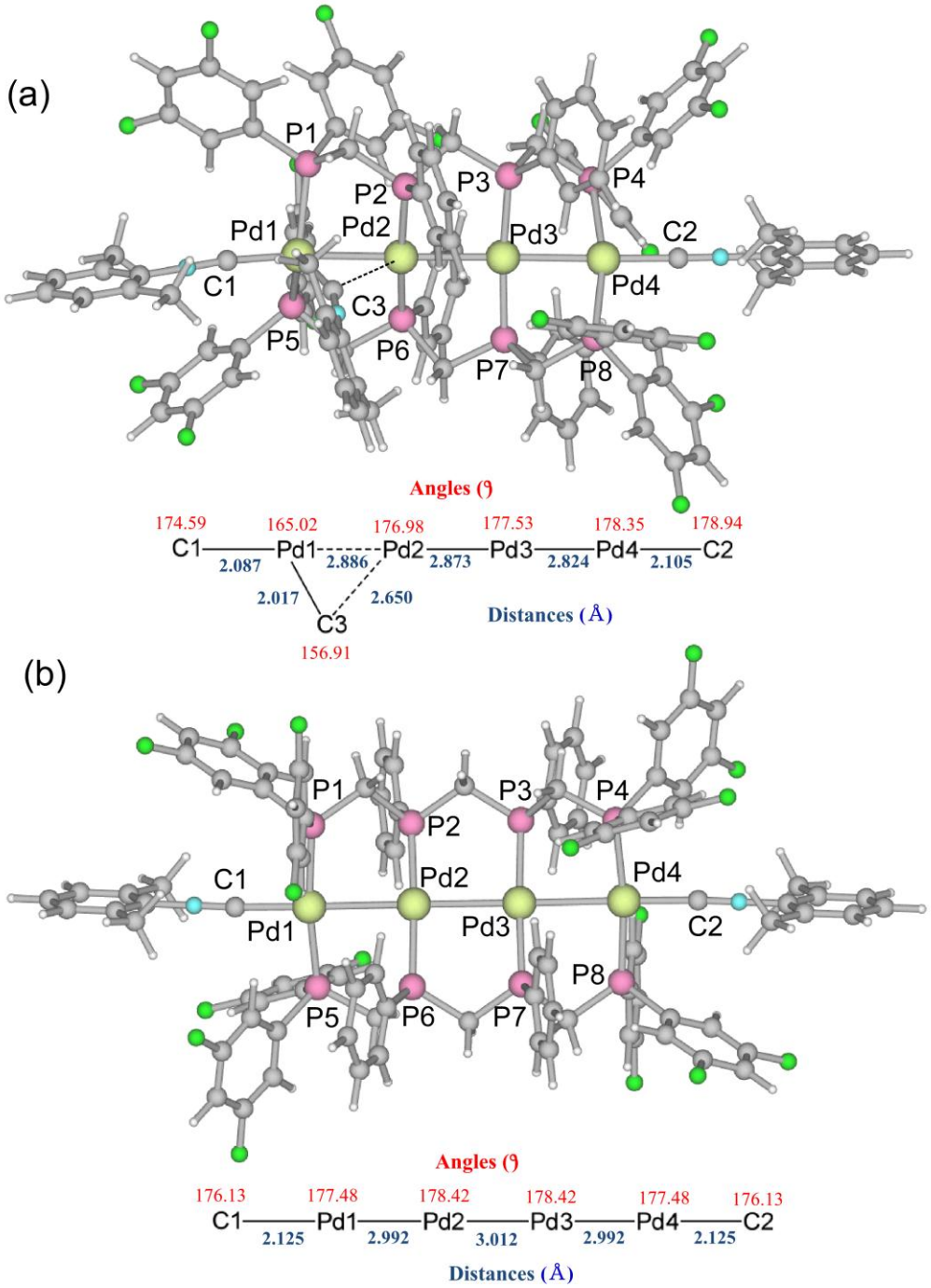

Fig. S10 Values of natural charge (red) and Wiberg bond indices (blue) derived from Natural Bond Analyses on the DFT optimized structures of (a) $[Pd_4(\mu\text{–}dpmppmF_2)_2(XylNC)_3]^{2+}$ (**1**) and (b) $[Pd_4(\mu\text{–}dpmppmF_2)_2(XylNC)_2]^{2+}$ (**1'**).